# Respiratory and intestinal epithelial cells exhibit differential susceptibility and innate immune responses to contemporary EV-D68 isolates

Megan Culler Freeman[1], Alexandra I. Wells[1, 2], Jessica Ciomperlik-Patton[4], Michael M. Myerburg[3], Jennifer Anstadt[4], and Carolyn B. Coyne[1,2,*]

[1]Department of Pediatrics, Division of Infectious Diseases, UPMC Children's Hospital of Pittsburgh, Pittsburgh, PA, USA,[2]Center for Microbial Pathogenesis, UPMC Children's Hospital of Pittsburgh, Pittsburgh, PA, USA,[3]Pulmonary, Allergy and Critical Care Medicine, University of Pittsburgh School of Medicine, Pittsburgh, PA [4] Division of Viral Diseases, Centers for Disease Control and Prevention, Atlanta, GA

Keywords: Enterovirus D68, airway, enteroid, interferon

Running Title: EVD68 infection in respiratory and intestinal epithelium

*Corresponding author
Carolyn Coyne, PhD
9116 Rangos Research Center
UPMC Children's Hospital of Pittsburgh
One Children's Hospital Way
4401 Penn Avenue
Pittsburgh, PA 15224
Phone (412) 692-7519
Email coynec2@pitt.edu

**Abstract:**

Enterovirus D68 (EV-D68) has been implicated in outbreaks of severe respiratory illness and acute flaccid myelitis (AFM) and is detected in patient respiratory samples and from stool and wastewater, suggesting both respiratory and enteric routes of transmission. Here, we used a panel of EV-D68 isolates, including a historical isolate and multiple contemporary isolates from AFM outbreak years, to define the dynamics of viral replication and the host response to infection in primary human airway cells and stem cell-derived enteroids. We show that some recent EV-D68 isolates have decreased sensitivity to acid and temperature compared with an earlier isolate and that the respiratory, but not intestinal, epithelium induces a robust type III interferon (IFN) response that restricts infection. Our findings define the differential responses of the respiratory and intestinal epithelium to contemporary EV-D68 isolates and suggest that some isolates have the potential to target both the human airway and gastrointestinal tracts.

## Introduction

Enteroviruses (EVs) are a family of positive-stranded RNA viruses, including coxsackieviruses, echoviruses, enterovirus A71 (EV-A71), and enterovirus D68 (EV-D68) that are responsible for a broad spectrum of illness in humans. EVs, specifically EV-D68 and EV-A71, have been associated with acute flaccid myelitis (AFM), a polio-like illness causing paralysis in previously healthy individuals, primarily children, which has peaked in even numbered years from at least 2014 until 2018 (Messacar et al., 2015; Midgley et al., 2015; Mishra et al., 2019; Schubert et al., 2019). While 2020 was anticipated to be a peak year for AFM, to date there has not been a surge of cases reported, perhaps indicating that coronavirus infection-control measures such as social distancing and mask usage have also diminished exposure to other circulating pathogens (CDC, 2020). While EVs are traditionally spread via the fecal-oral route, previous work with EV-D68 isolates before the AFM outbreak in 2014 suggested reduced replication in acidic environments and improved replication at lower temperature than traditional EVs, suggesting suitability for respiratory tract replication (Oberste, 2004).

EV-D68 has undergone rapid evolution since the 1990s, leading to the emergence of four clades, termed A-D (Du et al., 2015; Tokarz et al., 2012). This degree of evolution has led to loss of neutralization from pre-existing antibodies, highlighting the potential significance of these changes (Imamura et al., 2014). Contemporary EV-D68 isolates exhibit different biologic properties than historical reference isolates, including replication in neuronal cells (Brown et al., 2018). EV-D68 is often detected in patient respiratory samples, however, EV-D68 has also been isolated from stool specimens and wastewater, suggesting that it may also be transmitted by the fecal-oral route (Bisseux et al., 2018; Pham et al., 2017; Weil et al., 2017). The viral and host determinants that influence EV-D68 tropism remain largely unknown, particularly in the respiratory and gastrointestinal epithelium. Moreover, whether there are differences in the replication dynamics and/or host responses to isolates circulating prior to AFM outbreaks versus contemporary isolates is also unclear.

The EV-D68 reference isolate Fermon is often used as a historic isolate, due to its isolation in the mid-1960s. However, this isolate has undergone decades of passage through cell lines and has thus likely undergone changes that make it well-adapted for replication in cell culture and less representative of its original sequence when it was isolated from a child with pneumonia (Schieble et al., 1967). These changes highlight the need to perform comparative studies using pre-outbreak and contemporary EV-D68 isolates in order to define the viral and host determinants of infection. In this study, we performed comparative studies of replication kinetics, temperature sensitivity, polarity of infection, and cellular responses to infection using a panel of EV-D68 isolates, including a historic isolate and multiple isolates from AFM outbreak years. To define host cell-type specific differences in EV-D68 replication and/or host responses, we performed comparative studies in primary human bronchial epithelial (HBE) cells grown at an air-liquid interface and in primary human stem-cell derived intestinal enteroids. We found that respiratory and intestinal cell lines were permissive to both historic and contemporary EV-D68 isolates, but that there were isolate-specific differences in temperature sensitivity at 33°C or 37°C. In contrast, primary HBE cells were largely resistant to EV-D68 replication, with only one isolate, KY/14/18953, able to replicate. KY/14/18953 and MA/18/23089 were able to replicate in human enteroids. Primary HBE, but not enteroids, mount a robust innate immune response to EV-D68 infection, characterized by the induction of type III interferons (IFNs) and to a lesser extent type I IFNs. Lastly, we show that inhibition of IFN signaling enhances EV-D68 replication in primary HBE, supporting a role for this signaling in the control of viral replication in the airway. Collectively, these data define the differential responses of the respiratory and intestinal epithelium to historic and contemporary EV-D68 isolates.

## Results

### EV-D68 replication in lung and intestinal cell lines varies with isolate and temperature

We sought to evaluate the replication competency of a panel of EV-D68 isolates, including a historical 2009 isolate and five contemporary isolates from outbreaks in the AFM peak years of 2014 and 2018 in cell lines representing the respiratory and intestinal tracts (details of viral isolates can be found in **Supplemental Table 1**). To do this, we used the MD/09/23229 isolate, collected in 2009 and in clade A, as a reference isolate prior to the 2014 outbreak and multiple isolates associated with AFM outbreak seasons, including 2014 and 2018. These isolates are inclusive of multiple clades, B1, B2, B3, and D1, (Du et al., 2015; Hadfield et al., 2018; Sagulenko et al., 2018; Sun et al., 2019) that have been associated with peak-year AFM outbreaks. In addition, KY/14/18953 and US/IL/18952 isolates are paralytogenic in mouse models (Brown et al., 2018; Hixon et al., 2017). We evaluated replication at 33°C and at 37°C in Calu-3 cells, a lung adenocarcinoma cell line and in Caco-2 cells, a colon adenocarcinoma cell line. We found that while all isolates replicated to some degree at 33°C in Calu-3 cells, two isolates, MD/09/23229 and MA/18/23089, were unable to efficiently replicate at 37°C (**Figure 1A**). In Caco-2 cells, all isolates were able to replicate at 33°C (**Figure 1B**). When infections were performed at 37°C, MA/18/23089 and KY/14/18953 continued to replicate well over background in Caco-2 cells (**Figure 1B**). In contrast, infections in Calu-3 cells performed at 37°C severely restricted the replication of several isolates, including MD/09/23229, IL/14/18952, and MO/14/18949, whereas the replication of KY/14/18953 was less severely restricted (**Figure 1A**). Collectively, these studies suggest that select EV-D68 isolates exhibit cell type-specific sensitivity to temperature in cell lines (summarized in **Figure 1C**).

**Some contemporary EV-D68 isolates have increased acid tolerance**

We found that all EV-D68 isolates were capable of replicating in gastrointestinal-derived cell lines. However, in addition to cellular tropism, enteric viruses must be stable in acidic environments to infect the GI tract. Previous work suggested that select EV-D68 isolates were destabilized

following exposure to low pH (pH 4-6) as a mechanism of genome release during vial entry (Liu et al., 2018). However, whether this instability might influence the enteric route of transmission is unclear. In order to define the stability of EV-D68 virions in various conditions that mimic the environment in the GI tract, we exposed historical and contemporary isolates of EV-D68 to simulated intestinal fluids of the stomach and fed and fasted states of the small intestine over short (30 min) and long (60-120 min) exposure times. These fluids reflect not only the differential pH of the GI tract, but also contain bile acid and phospholipids that better recapitulate some aspects of the GI luminal content. To compare the stability of EV-D68 to other members of the enterovirus family that are transmitted primarily via the fecal-oral route, we performed similar studies with echovirus 11 (E11) and EVA71. E11 and EVA71 were stable in both fed state small intestine (FeSSIF pH 5) and fasted state small intestine (FaSSIF pH 6.5) for all exposure times tested (**Figure 2A, 2B**). However, whereas E11 exhibited significant reductions in titer when exposed to fasted state simulated gastric fluid (FaSSGF pH 2.0), EV71 was less impacted by this exposure (**Figure 2A, 2B**). None of the EV-D68 isolates tested were able to withstand the most acidic fluid (FaSSGF, pH 2.0) (**Figure 2C-F**). However, whereas EV-D68 isolates were generally stable in FaSSIF pH 6.5 conditions (**Figure 2C-F**), there were isolate-specific differences in stability in FeSSIF pH 5 conditions, with KY/14/18953 and to a lesser extent MA/18/23089 exhibiting some stability in this condition (**Figure 2D-F**). These data suggest that some contemporary isolates of EV-D68 exhibit enhanced stability in low pH conditions.

**Comparison of EV-D68 growth characteristics in primary human airway epithelial cells and stem cell-derived enteroids**

We found that many EV-D68 isolates efficiently infected airway- and intestinal-derived cell lines, which occurred in a temperature-dependent manner **(Figure 1)**. However, given that cell lines do not fully recapitulate the complexities of the airway and intestinal epithelium, we performed similar studies in primary cell models. To model the human airway, we used primary human bronchial

epithelial cells (HBE) grown at an air liquid interface (ALI). HBE have increased similarity to the human respiratory tract with respect to polarization, functional cilia, and mucus production than cell line-derived respiratory models and thus provide a more physiological system to study EV-D68 infections in the human airway. We infected HBE cells from at least two independent donors from either the apical (**Figure 3A, C, E, G**) or basolateral (**Figure 3B, D, F, H**) domains and measured viral titers in the apical (**Figure 3A-D**) and basolateral (**Figure 3E-H**) supernatants to determine whether EV-D68 exhibited a polarity of entry and/or release. We found that one isolate, KY/14/18953, infected similarly from the apical and basolateral domains at 33°C or 37°C (**Figure 3A-D**), but exhibited preferential release from the apical surface (**Figure 3A-H**). In contrast, MD/09/23229 replicated more efficiently from the basolateral surface and exhibited a temperature preference for 33°C (**Figure 3A-D**). However, similar to KY/14/18953, it was also released preferentially from the apical surface (**Figure 3A-H**). Another contemporary isolate, IL/14/18952, infected best from the basolateral surface at 33°C while the contemporary isolate MA/18/23089 infected primary HBE inefficiently from either domain or temperature (**Figure 3A-H,** summarized in **3I**). These data suggest that some isolates exhibit a preferential polarity of infection and are released primarily via the apical surface.

Next, we determined whether EV-D68 could infect GI-derived primary cells, particularly given that all isolates replicated to high titers in a GI-derived adenocarcinoma cell line (Caco-2). To do this, we used human primary stem cell-derived enteroids, which we used previously to define the cellular tropism of other enteroviruses in the GI epithelium (Drummond et al., 2017; Good et al., 2019). We found that only one isolate, KY/14/18953, replicated in human enteroids, which occurred in a temperature-independent manner but that there were very low levels of infection by other isolates tested, although MD/09/232229 exhibited some capacity to replicate to low levels (**Figure 4A-B**). A limitation of the above-described model is that enteroids grown in Matrigel exhibit an “inside out” polarity, with the luminal surface facing inward. As we have previously shown that some enteroviruses such as EV-A71 exhibit preferential infection of the

188 apical domain, we next determined whether EV-D68 exhibited a similar polarity, which might
189 explain the low levels of infection in enteroids grown in Matrigel (Good et al., 2019). To address
190 this, we cultured intestinal crypts on Transwell inserts, which allows for the development of a
191 monolayer containing diverse intestinal cell types (Good et al., 2019). Similar to our studies in
192 HBE, we infected intestinal monolayers from the apical (**Figure 4C, 4E**) or basolateral (**Figure**
193 **4D, 4F**) domains and sampled the apical (**Figure 4C-D**) or basolateral (**Figure 4E-F**) supernatant
194 for infectious virus. We found that KY/14/18953 replicated to high titers when inoculated from
195 either the apical or basolateral surfaces but exhibited a preferential release into the apical
196 compartment (**Figure 4C-F**), similar to what was observed in primary HBE. In contrast to our
197 findings in Matrigel-derived enteroids, we found that MA/18/23089 replicated to high titers when
198 infection was initiated from the apical surface, with slightly lower titers from the basolateral domain
199 (**Figure 4C-F**). However, similar to KY/14/18953, this isolate also exhibited preferential release
200 into the apical compartment (**Figure 4C-F**). Collectively, these data show that some contemporary
201 isolates of EV-D68, particularly KY/14/18953, can replicate to higher titers in both primary HBE
202 and enteroids (summarized in **Figure 3I** and **4G**). In contrast, the historical isolate MD/09/23229
203 replicated to low titers in primary HBE, which only occurred at 33ºC and was unable to replicate
204 in enteroids (**Figure 3I** and **4G**).
205
206 **EV-D68 infection induces cell type-specific antiviral signaling**
207 To define the cellular response to EV-D68 infection in HBE and in enteroids, we first performed
208 RNAseq-based whole transcriptional profiling using select EV-D68 isolates, the historic strain
209 MD/09/23229 and, due to successful replication under all tested conditions, KY/14/18953.
210 Consistent with our infectious titer data, HBE cells infected from the basolateral surface had
211 higher viral RNA (vRNA) fragments per kilobase per million reads mapped (FPKM) reads than
212 those infected apically (**Supplemental Figure 1A**). However, despite near-equivalent viral input,
213 HBE cells infected with MD/09/23229 had higher vRNA FPKM values than those infected with

KY/14/18953 (**Supplemental Figure 1A**), despite higher infectious titers in cells infected with KY/14/18953. We found that vRNA FPKM values in enteroids infected with KY/14/18953 were significantly higher than those observed in HBE and that these values were independent of temperature, as we obtained similar values in enteroids infected at 33°C or 37°C (**Supplemental Figure 1A**). Next, we performed differential expression analysis to identify transcripts induced by EV-D68 infection. Despite significant differences in the levels of infection, HBE infected with either MD/09/23229 or KY/14/18953 from the basolateral surface induced similar numbers of transcripts, with MD/09/23229 inducing 178 (**Supplemental Figure 1B, Supplemental Table 3**) and KY/14/18953 inducing 189 (**Supplemental Figure 1C, Supplemental Table 3**). Consistent with the low levels of vRNA present in HBE infected from the apical surface, relatively very few transcripts were induced under these conditions, with MD/09/23229 inducing 37 (**Supplemental Figure 1B, Supplemental Table 3**) and KY/14/18953 inducing 30 (**Supplemental Figure 1C**, **Supplemental Table 1B).** Of the transcripts induced by basolateral infection, approximately half were shared between HBE infected with MD/09/23229 or KY/14/18953 (92 total, **Supplemental Table 4)**. These transcripts were enriched in interferon stimulated genes (ISGs) (**Supplemental Figure 1F**, **Supplemental Table 4**). In contrast, there were very few transcripts induced by both HBE and enteroids infected with KY/14/18953, with only 9 transcripts shared between these conditions, despite enteroids inducing a greater total number of transcripts (332 total) (**Supplemental Figure 1E**, **Supplemental Table 5)**. Of these transcripts, five included ISGs (MX2, IFIT3, IFIT1, IFI27, and IFITM1), which were induced in all conditions tested (**Supplemental Figure 1G**). Consistent with the induction of ISGs, HBE infected with MD/09/23229 or KY/14/18953 from the basolateral surface, and to a lesser extent the apical surface, potently induced the expression of the type III IFNs IFN-l1-3, but not type I or II IFNs (**Supplemental Figure 1H**). In contrast, KY/14/18953 infection of enteroids elicited no significant induction of these transcripts, despite the higher levels of vRNA present in these samples

(**Supplemental Figure 1A, 1H**). Taken together, these data suggest that there are cell type-specific differences in the response of HBE and enteroids to EV-D68 infection.

**EV-D68 infection of primary human airway cells preferentially induces type III IFNs**

Our RNASeq-based studies pointed to cell type-specific differences in the response of primary HBE and enteroids to EV-D68 infection. To further define the cellular response to EV-D68 infection, we performed multianalyte Luminex-based assays for 37 pro-inflammatory cytokines in cells infected with historical and contemporary EV-D68 isolates at 33ºC at both 24h and 48h post-infection. In HBE, we also directly compared the impact of the polarity of infection on cytokine induction. At 24h p.i., all EV-D68 isolates induced the type III IFNs IFN-λ1 and IFN-λ2, with little to no significant induction of the type I IFNs IFN-β and IFN-α2 (**Figure 5A-G**). Of note, despite the low levels of viral replication in HBE infected from the apical surface (**Figure 3**), we observed near-equivalent levels of IFN induction under these conditions (**Figure 5A-G**). At 48h p.i., levels of type III IFNs further increased to very high levels (>10ng/mL) (**Figure 5A, 5D-G**). In addition, at the later time point, we observed a significant induction of IFN-β, but not IFN-α2 (**Figure 5A-C**). In contrast to EV-D68-infected HBE, EV-D68 infection in enteroids did not induce detectable changes in any of the cytokines tested, including IFNs (**Figure 5A, 5D-G).** These data suggest that the airway and intestinal epithelium induce cell type-specific responses to EV-D68 infection.

Prior reports have suggested that *in vitro* respiratory virus replication differences at 33°C and 37°C may be related to increased IFN responses at higher temperatures (Foxman et al., 2015). To determine whether differential temperature-dependent IFN responses explained differences in EV-D68 replication in HBE at 33ºC and 37ºC, we again utilized Luminex-based multiplex assays against 37 pro-inflammatory cytokines, including type I and III IFNs. To do this, we compared infection of primary HBE cells with EV-D68 isolates MD/09/23229 and KY/14/18953 at 33ºC and 37ºC for either 24 or 48 hpi. Despite differences in the efficiency of replication in HBE

264 at 33°C and 37°C, we did not detect any significant differences in the induction of type I (IFN-β)
265 or III (IFN-λ1, IFN-λ2) IFNs under these conditions (**Supplemental Figure 2A-D**). In addition, we
266 found that Calu-3 lung epithelial and Caco-2 intestinal epithelial cell lines did not mount an IFN-
267 mediated immune response to EV-D68 infection at either temperature (**Supplemental Figure 2E-**
268 **F**).
269
270 **IFN signaling restricts EV-D68 replication in primary human airway cells**
271 We observed robust IFN-mediated antiviral signaling in HBE cells infected with EV-D68 despite
272 very low to undetectable levels of replication, suggesting that this antiviral response restricts EV-
273 D68 infection. To test this, we infected HBE cells with EV-D68 in the presence of a selective small-
274 molecule inhibitor of JAK1/2 signaling (ruxolitinib). Treatment of HBE with ruxolitinib significantly
275 decreased the secretion of IFN-b and IFN-l1 in response to EV-D68 infection (**Figure 6A-B**) and
276 also significantly reduced ISG induction (**Figure 6C)**. Consistent with this, there was a significant
277 increase in MD/09/23229 infectious titers at 48 hpi as compared to DMSO-treated controls, with
278 less robust enhancement of KY/14/18953 (**Figure 6D**).
279
280 **Discussion**
281 In this study, we define differences in the dynamics of EV-D68 replication and pH stability using
282 a panel of isolates from AFM peak years and a pre-outbreak isolate. In addition, utilizing two
283 primary human cell models representing common tissue sites targeted by enteroviruses in
284 humans, we define differences in epithelial responses to EV-D68 between the respiratory and GI
285 tracts. Collectively, this work details the varied responses of the respiratory and intestinal
286 epithelium to historic and contemporary EV-D68 isolates and defines the role of type III IFN
287 signaling in the control of EV-D68 infection in the respiratory, but not intestinal, epithelium.

We found that most isolates of EV-D68 efficiently replicated in both respiratory and intestinal epithelial cell lines, although there were some isolate-specific differences in temperature sensitivity. By comparison, primary HBE cells were less permissive to EV-D68 infection. One isolate, KY/14/18953, replicated very efficiently in primary HBE from either the apical or basolateral domains at both 33°C and 37°C, but exhibited a preferential release into the apical compartment. Another isolate, IL/14/18952, infected preferentially from the basolateral surface, but similarly was released into the apical compartment. The historic isolate MD/09/23229 and contemporary isolate MA/18/23089 replicated to comparably lower levels in all conditions but shared an apical release preference. Despite high levels of infection in the intestinal-derived Caco-2 cell line, only one isolate, KY/14/18953, replicated to high titers in stem cell-derived enteroids, although the contemporary isolate MA/18/23089 also replicated to low, but detectable, levels which improved when access to the apical surface was available. These studies point to key differences in the susceptibility of different primary epithelial-derived cell models to EV-D68 infection and suggest that host factors likely influence this tropism. For example, although attachment factors have been identified for EV-D68, including sialic acid and decay accelerating factor (DAF), some contemporary strains of EV-D68 including KY/14/18953 do not bind to sialylated receptors and their role in mediating infection is unknown (Baggen et al., 2016; Blomqvist et al., 2002). In addition, the neuron-specific intercellular adhesion molecule 5 (ICAM-5/telencephalin) has been identified as a potential receptor for several historic and contemporary isolates of EV-D68, but restricted expression in other cell types makes it unclear what role it might play in the epithelium (Hixon et al., 2019; Wei et al., 2016).

Previous work with EV-D68 before the emergence of AFM suggested that due to preferences for replication at 33°C and sensitivity to acid *in vitro*, it was more suited to be a respiratory pathogen behaving similarly to rhinoviruses as opposed to other enteroviruses (Liu et al., 2018; Oberste, 2004). While previous studies have evaluated acid stability of EV-D68, we utilized biologically relevant solutions with complexities other than acidity, such as bile acid and

phospholipids, that more closely mimic the gastrointestinal environment. Our studies using multiple contemporary isolates after the emergence of AFM suggest that these isolates are relatively stable at 37°C and also have improved acid stability. However, none of the EV-D68 isolates tested were stable during even short incubations with the most acidic fluid, the simulated fasted state stomach fluid, at a pH of 2. Our data also indicate that many isolates of EV-D68, even those associated with AFM outbreaks, are unable to replicate efficiently in human enteroids. However, one contemporary isolate, KY/14/18953, replicated to high levels in human enteroids and we observed replication of the contemporary isolate MA/18/23089 when primary intestinal enteroids were cultured on Transwell inserts. The basis for the very high capacity of KY/14/18953 to replicate in enteroids is unknown, but this isolate is genetically unique, and it is one of the very few members of the newly defined clade D, which thereby exhibits significant sequence variation in the VP1 region often used for receptor binding. These data suggest that the intestinal epithelium might serve as a site of EV-D68 transmission, particularly for some isolates.

The pro-viral factors that mediate EV-D68 infection in the epithelium remain largely unknown, but our studies suggest that the induction of IFN signaling plays a major role in restricting replication in the airway epithelium. We have shown previously that type III IFNs are preferentially induced by enterovirus infections in human enteroids and that this signaling restricts replication (Drummond et al., 2017; Good et al., 2019). In addition, type III IFNs are also the dominant IFNs induced in response to influenza, RSV, measles, and mumps infections of respiratory epithelial cells (Crotta et al., 2013; Fox et al., 2015; Galani et al., 2017; Jewell et al., 2010; Okabayashi et al., 2011). Although the type I IFN IFN-b was induced in response to EV-D68 infection, its induction was delayed compared to type III IFNs. Of note, we observed significant induction of IFNs even when levels of infection were not detectable, highlighting the potency by which the airway epithelium responds to these infections. The induction of IFNs is likely one mechanism by which the airway restricts EV-D68 replication, which is supported by our findings that treatment of HBE with ruxolitinib increased infection. However, it should be noted

that ruxolitinib only partially recovers infection, suggesting other cellular pathways in addition to IFN also restrict infection. Surprisingly, despite robust IFN induction in response to EV-D68 infection of primary HBE, primary human enteroids did not mount any detectable IFN response to EV-D68 infection, suggesting that there are important differences in the capacity of the respiratory and airway epithelium to sense and respond to EV-D68 infection. The lack of antiviral signaling in infected enteroids would appear to be specific for EV-D68, as we have shown previously that enteroids infected with other enteroviruses including CVB, echoviruses, and EV71 respond via the induction of type III IFNs (Drummond et al., 2017; Good et al., 2019). While the mechanistic basis for this is unknown, differences in viral antagonism strategies and/or host detection mechanisms may explain these differences.

Currently there are no available no virus-specific treatments or vaccines to prevent AFM, which is a critically important emerging illness with significant morbidity to young children. Further understanding how EV-D68 targets the airway and/or gastrointestinal epithelium are critical to improve our understanding of how is transmitted, particularly given increases in its circulation. Our work presented here provides important insights into the dynamics of EV-D68 replication in the human airway and intestinal epithelium and provide ideal models to develop and test anti-EV-D68 therapeutics.

## Materials and Methods

*Cell culture*

HeLa cells were provided by Dr. Jefferey Bergelson, Children's Hospital of Philadelphia, Philadelphia, PA, and grown in MEM, with 5% FBS, non-essential amino acids, and penicillin/streptomycin. Calu-3 cells (HTB-55) were obtained from the ATCC grown in MEM w/ 10% FBS and 1% pen/strep and Caco-2 cells (BBE clone, CRL-2101) were obtained from the ATCC and grown in DMEM with 10% FBS and 1% pen/strep.

366 *Human intestinal enteroids*

367 Human intestinal enteroid lines were derived as previously described by isolation of intestinal
368 crypts from small intestine (Drummond et al., 2017) obtained from the University of Pittsburgh
369 Biospecimen Core through an honest broker system after approval from the University of
370 Pittsburgh Institutional Review Board and in accordance with the University of Pittsburgh
371 anatomical tissue procurement guidelines and frozen. Enteroid lines were thawed, passaged, and
372 maintained as previously described (Stewart et al., 2020) in Matrigel. Experiments with enteroids
373 were performed on a Matrigel coating or on Transwell inserts, as detailed in the text. Crypt culture
374 medium was composed of Advanced DMEM/F12 (Invitrogen) with 20% HyClone ES (embryonic
375 stem) Cell Screened Fetal Bovine Serum (Thermo Fisher Scientific), 1% penicillin/streptomycin
376 (Invitrogen), 1% L-glutamine, 1% *N*-acetylcysteine (100 mM; Sigma-Aldrich), 1% N-2 supplement
377 (100×; Invitrogen), 2% B27 supplement (50×; Invitrogen), Gibco Hepes (*N*-2-
378 hydroxyethylpiperazine-*N*-2-ethane sulfonic acid, 0.05 mM; Invitrogen), ROCK Inhibitor Y-27632
379 (1 mM, 100×; Sigma) and supplemented with the following growth factors: WNT3a, R-spondin,
380 and Noggin as produced by preconditioned media from WRN cells obtained from the ATCC (CRL-
381 3276) and described previously (Miyoshi and Stappenbeck, 2013) and hEGF (50 ng/ml; Thermo
382 Fisher Scientific) (Egan et al., 2016; Shaffiey et al., 2016) and was changed every 48-72 hours
383 throughout culturing.
384
385 *Human Bronchial Epithelial Cells (HBE)*
386 Primary HBE cells were differentiated from human lung tissue by following an IRB–approved
387 protocol and were maintained at an air-liquid interface with differentiation media changed twice
388 per week, as described previously (Myerburg et al., 2010). Differentiation media (BEGM/Ultroser
389 G; Pall Corporation, Crescent Chemical Company, Islandia, NY) was comprised of 5 µg/ml insulin,
390 10 µg/ml transferrin, 0.07 µg/ml hydrocortisone, 0.6 µg/ml epinephrine, 0.8% vol/vol bovine
391 hypothalamus extract, 0.5 mg/mL BSA, 0.5 µM ethanolamine, 15 ng/ml retinoic acid, 0.5 ng/ml

392 human epidermal growth factor, 10 nM triiodothyronine, 0.5 μM phosphoethanolamine, and 0.5%
393 vol/vol Ultroser G (USG) in Dulbecco's MEM (DMEM)/F12. Cells were cultured for 3-6 weeks in
394 order to differentiate and achieve a mucociliary phenotype on phase contrast microscopy prior to
395 all experiments. Mucus was removed by extensive washes in 1x PBS prior to infection.
396
397 *Viruses and Infections*

398 Experiments were performed with a panel of EV-D68 viruses described in **Supplemental Table**
399 **1**. Viruses were grown in HeLa cells at 33°C in 5% $CO_2$ until CPE was observed, purified by
400 ultracentrifugation over a 30% sucrose cushion as previously described (Morosky et al., 2016).
401 Purity of all viral stocks was confirmed by Sanger sequencing of VP1 using enterovirus-specific
402 primers, as described previously (Oberste et al., 2003). Plaque assays were performed in HeLa
403 cells overlayed with 1% agarose, incubated for 72 h, and plaques counted after staining with
404 crystal violet. Viruses were obtained from the ATCC or were provided by the Center for Disease
405 Control and Prevention (CDC) as noted in **Supplemental Table 1**.

406 For infections, cells were infected with $10^6$ plaque-forming units (PFU) of indicated viral
407 isolates. Virus was adsorbed to the cell surface (apical or basolateral as indicated) for 1 hour at
408 room temperature, cells were then washed with PBS, and then media replaced prior to placement
409 back in the incubator at the indicated temperature for the indicated times. For viral replication
410 analysis, aliquots of media were collected at indicated times post-infection and virus was detected
411 via TCID50 assays in HeLa cells. For HBE growth experiments, media was applied to the apical
412 surface at the indicated timepoint and incubated for 30 minutes at the experimental temperature
413 prior to collection.

414 *Simulated intestinal fluids*

Simulated gastric fluid powders fasted state gastric fluid (FaSSGF), fasted state small intestinal fluid (FaSSIF), and fed state small intestine (FeSSIF) (Biorelevant) were prepared as described by the manufacturer. $10^6$ PFU/mL of the indicated virus was incubated in FaSSGF, FaSSIF, FeSSIF, or DMEM for the indicated time at 37°C. A one mL aliquot was collected, neutralized to pH 7.0 with 2.5M sodium hydroxide, and then replication competence was assessed via TCID50 assay.

*qPCR*

Total RNA was isolated from cells using the Sigma GenElute Total Mammalian RNA Miniprep Kit, according to the manufacturer protocol with the addition of a Sigma DNase digest reagent. RNA (1mg total) was reverse transcribed using iScript cDNA Synthesis Kit (Bio-Rad) and diluted to 100 µl in ddH20 for subsequent qPCR. RT-qPCR was performed using the iQ SYBR Green Supermix or iTaq Universal SYBR Green Supermix (Bio-Rad) on a CFX96 Touch Real-Time PCR Detection System (Bio-Rad). Gene expression was determined on the basis of a $\Delta C_Q$ method, normalized to human actin. Primer sequences can be found in **Supplemental Table 2**.

*RNASeq*

Total RNA was extracted as described above. RNA quality and concentration were determined by NanoDrop, then 1 µg of RNA was used for library preparation with TruSeq Stranded mRNA Library Preparation Kit (Illumina) per the manufacturer's instructions. Illumina NextSeq 500 was used for sequencing. RNA-seq FASTQ data were processed and mapped to the human reference genome (hg38) with the CLC Genomics Workbench 20 (Qiagen). Differential gene expression was analyzed with the DESeq2 package in R (Drummond et al., 2015). Raw sequencing files have been deposited in Sequence Read Archives and are publicly available (PRJNA688898).

*Luminex assays*

Luminex profiles utilized the Human Inflammation Panel 1 37-plex assay kit (Bio-Rad) per the manufacturer's protocol using the laboratory multianalyte profiling system (MAGPIX) developed by Luminex Corporation (Austin, TX).

*Inhibitor treatments*

HBE cells or enteroids on MG coats were incubated with 5 μM ruxolitinib or dimethyl sulfoxide (DMSO) control for 1 hour at 37°C and then infected with the indicated EV-D68 isolate in the presence of ruxolitinib or DMSO.

*Statistics*

Statistical analysis was performed with GraphPad Prism software version 8.4.3. Experiments were performed at least three times and primary cells from at least two genetically distinct donors were utilized for each experiment. Data are presented as mean ± standard deviation. Student's *t* test or one-way analysis of variance (ANOVA) was used to determine significance, as indicated in figure legends, for normally distributed data. Growth curve analysis was completed using two-way ANOVAs. *P* values of $<0.05$ was considered significant and are indicated in the figure legends.

## References

Baggen, J., Thibaut, H.J., Staring, J., Jae, L.T., Liu, Y., Guo, H., Slager, J.J., Bruin, J.W. de, Vliet, A.L.W. van, Blomen, V.A., et al. (2016). Enterovirus D68 receptor requirements unveiled by haploid genetics. Proc National Acad Sci *113*, 1399–1404.

Bisseux, M., Colombet, J., Mirand, A., Roque-Afonso, A.-M., Abravanel, F., Izopet, J., Archimbaud, C., Peigue-Lafeuille, H., Debroas, D., Bailly, J.-L., et al. (2018). Monitoring human enteric viruses in wastewater and relevance to infections encountered in the clinical setting: a one-year experiment in central France, 2014 to 2015. Eurosurveillance *23*, 17–00237.

Blomqvist, S., Savolainen, C., Raman, L., Roivainen, M., and Hovi, T. (2002). Human Rhinovirus 87 and Enterovirus 68 Represent a Unique Serotype with Rhinovirus and Enterovirus Features. Journal of Clinical Microbiology *40*, 4218–4223.

Brown, D.M., Hixon, A.M., Oldfield, L.M., Zhang, Y., Novotny, M., Wang, W., Das, S.R., Shabman, R.S., Tyler, K.L., and Scheuermann, R.H. (2018). Contemporary Circulating Enterovirus D68 Strains Have Acquired the Capacity for Viral Entry and Replication in Human Neuronal Cells. MBio *9*, 2508–2517.

CDC (2020). AFM Cases and Outbreaks. 2 Dec. 2020, www.cdc.gov/acute-flaccid-myelitis/cases-in-us.html.

Crotta, S., Davidson, S., Mahlakoiv, T., Desmet, C.J., Buckwalter, M.R., Albert, M.L., Staeheli, P., and Wack, A. (2013). Type I and Type III Interferons Drive Redundant Amplification Loops to Induce a Transcriptional Signature in Influenza-Infected Airway Epithelia. Plos Pathog *9*, e1003773.

Drummond, C.G., Nickerson, C.A., and Coyne, C.B. (2015). A Three-Dimensional Cell Culture Model To Study Enterovirus Infection of Polarized Intestinal Epithelial Cells. MSphere *1*, e00030-15–17.

Drummond, C.G., Bolock, A.M., Ma, C., Luke, C.J., Good, M., and Coyne, C.B. (2017). Enteroviruses infect human enteroids and induce antiviral signaling in a cell lineage-specific manner. Proceedings of the National Academy of Sciences *114*, 1672–1677.

Du, J., Zheng, B., Zheng, W., Li, P., Kang, J., Hou, J., Markham, R., Zhao, K., and Yu, X.-F. (2015). Analysis of Enterovirus 68 Strains from the 2014 North American Outbreak Reveals a New Clade, Indicating Viral Evolution. Plos One *10*, e0144208.

Egan, C.E., Sodhi, C.P., Good, M., Lin, J., Jia, H., Yamaguchi, Y., Lu, P., Ma, C., Branca, M.F., Weyandt, S., et al. (2016). Toll-like receptor 4–mediated lymphocyte influx induces neonatal necrotizing enterocolitis. J Clin Invest *126*, 495–508.

Fox, J.M., Crabtree, J.M., Sage, L.K., Tompkins, S.M., and Tripp, R.A. (2015). Interferon Lambda Upregulates IDO1 Expression in Respiratory Epithelial Cells After Influenza Virus Infection. J Interf Cytokine Res *35*, 554–562.

Foxman, E.F., Storer, J.A., Fitzgerald, M.E., Wasik, B.R., Hou, L., Zhao, H., Turner, P.E., Pyle, A.M., and Iwasaki, A. (2015). Temperature-dependent innate defense against the common cold

virus limits viral replication at warm temperature in mouse airway cells. Proc National Acad Sci *112*, 827–832.

Galani, I.E., Triantafyllia, V., Eleminiadou, E.-E., Koltsida, O., Stavropoulos, A., Manioudaki, M., Thanos, D., Doyle, S.E., Kotenko, S.V., Thanopoulou, K., et al. (2017). Interferon-λ Mediates Non-redundant Front-Line Antiviral Protection against Influenza Virus Infection without Compromising Host Fitness. Immunity *46*, 875-890.e6.

Good, C., Wells, A.I., and Coyne, C.B. (2019). Type III interferon signaling restricts enterovirus 71 infection of goblet cells. Sci Adv *5*, eaau4255.

Hadfield, J., Megill, C., Bell, S.M., Huddleston, J., Potter, B., Callender, C., Sagulenko, P., Bedford, T., and Neher, R.A. (2018). Nextstrain: real-time tracking of pathogen evolution. Bioinformatics *34*, 4121–4123.

Hixon, A.M., Yu, G., Leser, J.S., Yagi, S., Clarke, P., Chiu, C.Y., and Tyler, K.L. (2017). A mouse model of paralytic myelitis caused by enterovirus D68. PLOS Pathogens *13*, e1006199-19.

Hixon, A.M., Clarke, P., and Tyler, K.L. (2019). Contemporary circulating enterovirus D68 strains infect and undergo retrograde axonal transport in spinal motor neurons independent of sialic acid. Journal of Virology 1–39.

Imamura, T., Okamoto, M., Nakakita, S. -i, Suzuki, A., Saito, M., Tamaki, R., Lupisan, S., Roy, C.N., Hiramatsu, H., Sugawara, K. -e, et al. (2014). Antigenic and Receptor Binding Properties of Enterovirus 68. J Virol *88*, 2374–2384.

Jewell, N.A., Cline, T., Mertz, S.E., Smirnov, S.V., Flaño, E., Schindler, C., Grieves, J.L., Durbin, R.K., Kotenko, S.V., and Durbin, J.E. (2010). Lambda Interferon Is the Predominant Interferon Induced by Influenza A Virus Infection In Vivo ▿ . J Virol *84*, 11515–11522.

Liu, Y., Sheng, J., Vliet, A.L.W. van, Buda, G., Kuppeveld, F.J.M. van, and Rossmann, M.G. (2018). Molecular basis for the acid-initiated uncoating of human enterovirus D68. Proceedings of the National Academy of Sciences *115*, E12209–E12217.

Messacar, K., Schreiner, T.L., Maloney, J.A., MD, A.W., Ludke, J., Oberste, M.S., Nix, W.A., PhD, C.C.R., MD, M.P.G., MD, M.J.A., et al. (2015). A cluster of acute flaccid paralysis and cranial nerve dysfunction temporally associated with an outbreak of enterovirus D68 in children in Colorado, USA. The Lancet *385*, 1662–1671.

Midgley, C.M., Watson, J.T., Nix, W.A., Curns, A.T., Rogers, S.L., Brown, B.A., Conover, C., Dominguez, S.R., Feikin, D.R., Gray, S., et al. (2015). Severe respiratory illness associated with a nationwide outbreak of enterovirus D68 in the USA (2014): a descriptive epidemiological investigation. Lancet Respir Medicine *3*, 879–887.

Mishra, N., Ng, T.F.F., Marine, R.L., Jain, K., Ng, J., Thakkar, R., Caciula, A., Price, A., Garcia, J.A., Burns, J.C., et al. (2019). Antibodies to Enteroviruses in Cerebrospinal Fluid of Patients with Acute Flaccid Myelitis. Mbio *10*, e01903-19.

532 Miyoshi, H., and Stappenbeck, T.S. (2013). In vitro expansion and genetic modification of
533 gastrointestinal stem cells in spheroid culture. Nat Protoc *8*, 2471–2482.

534 Morosky, S., Lennemann, N.J., and Coyne, C.B. (2016). BPIFB6 Regulates Secretory Pathway
535 Trafficking and Enterovirus Replication. Journal of Virology *90*, 5098–5107.

536 Myerburg, M.M., Harvey, P.R., Heidrich, E.M., Pilewski, J.M., and Butterworth, M.B. (2010).
537 Acute Regulation of the Epithelial Sodium Channel in Airway Epithelia by Proteases and
538 Trafficking. Am J Resp Cell Mol *43*, 712–719.

539 Oberste, M.S. (2004). Enterovirus 68 is associated with respiratory illness and shares biological
540 features with both the enteroviruses and the rhinoviruses. Journal of General Virology *85*, 2577–
541 2584.

542 Oberste, M.S., Nix, W.A., Maher, K., and Pallansch, M.A. (2003). Improved molecular
543 identification of enteroviruses by RT-PCR and amplicon sequencing. J Clin Virol *26*, 375–377.

544 Okabayashi, T., Kojima, T., Masaki, T., Yokota, S., Imaizumi, T., Tsutsumi, H., Himi, T., Fujii, N.,
545 and Sawada, N. (2011). Type-III interferon, not type-I, is the predominant interferon induced by
546 respiratory viruses in nasal epithelial cells. Virus Res *160*, 360–366.

547 Pham, N.T.K., Thongprachum, A., Baba, T., Okitsu, S., Trinh, Q.D., Komine-Aizawa, S.,
548 Shimizu, H., Hayakawa, S., and Ushijima, H. (2017). A 3-Month-Old Child with Acute
549 Gastroenteritis with Enterovirus D68 Detected from Stool Specimen. Clin Lab *63*, 1269–1272.

550 Sagulenko, P., Puller, V., and Neher, R.A. (2018). TreeTime: Maximum-likelihood phylodynamic
551 analysis. Virus Evol *4*, vex042-.

552 Schieble, J.H., Fox, V.L., and Lennette, E.H. (1967). A probable new human picornavirus
553 associated with respiratory disease. Am J Epidemiol *85*, 297–310.

554 Schubert, R.D., Hawes, I.A., Ramachandran, P.S., Ramesh, A., Crawford, E.D., Pak, J.E., Wu,
555 W., Cheung, C.K., Donovan, B.D.O. x02019, Tato, C.M., et al. (2019). Pan-viral serology
556 implicates enteroviruses in acute flaccid myelitis. Nature Medicine 1–18.

557 Shaffiey, S.A., Jia, H., Keane, T., Costello, C., Wasserman, D., Quidgley, M., Dziki, J., Badylak,
558 S., Sodhi, C.P., March, J.C., et al. (2016). Intestinal stem cell growth and differentiation on a
559 tubular scaffold with evaluation in small and large animals. Regen Med *11*, 45–61.

560 Stewart, C.J., Estes, M.K., and Ramani, S. (2020). Innate Lymphoid Cells, Methods and
561 Protocols. Methods Mol Biology Clifton N J *2121*, 185–198.

562 Sun, J., Hu, X.-Y., and Yu, X.-F. (2019). Current Understanding of Human Enterovirus D68.
563 Viruses *11*, 490.

564 Tokarz, R., Firth, C., Madhi, S.A., Howie, S.R.C., Wu, W., Sall, A.A., Haq, S., Briese, T., and
565 Lipkin, W.I. (2012). Worldwide emergence of multiple clades of enterovirus 68. J Gen Virol *93*,
566 1952–1958.

567 Wei, W., Guo, H., Chang, J., Yu, Y., Liu, G., Zhang, N., Willard, S.H., Zheng, S., and Yu, X.-F.
568 (2016). ICAM-5/Telencephalin Is a Functional Entry Receptor for Enterovirus D68. Cell Host &
569 Microbe *20*, 631–641.

570 Weil, M., Mandelboim, M., Mendelson, E., Manor, Y., Shulman, L., Ram, D., Barkai, G.,
571 Shemer, Y., Wolf, D., Kra-oz, Z., et al. (2017). Human enterovirus D68 in clinical and sewage
572 samples in Israel. J Clin Virol *86*, 52–55.

573

574

## Acknowledgements

This work was supported by NIH R01- AI081759 (C.B.C.), the Children's Hospital of Pittsburgh of the UPMC Health System (C.B.C), NIH T32-AI060525 (A.I.W), NIH F31-AI149866 (A.I.W.), the Pediatric Infectious Diseases Society/St. Jude Research Hospital Fellowship in Basic and Translational Research (M.C.F), and the Cystic Fibrosis Foundation Research Development Program (University of Pittsburgh). All authors declare that they have no competing interests. All data needed to evaluate the conclusions in the paper are present in the paper and/or the Supplementary Materials. Additional data related to this paper may be requested from the corresponding author. The findings and conclusions in this report are those of the author(s) and do not necessarily represent the official position of the Centers for Disease Control and Prevention or other contributing agencies.

588 **Supplemental Table 1**: List of viral isolates used in the study

| Species | Isolate name | Abbreviation | D68 clade | Accession # | Source |
|---|---|---|---|---|---|
| Enterovirus D68 | USA/MD/2009-23229 | MD/09/23229 | A1 | MN240505 | CDC |
| Enterovirus D68 | US/MO/14-18949 | MO/14/18949 | B1 | KM851227 | CDC |
| Enterovirus D68 | US/IL/14-18952 | IL/14/18952 | B2 | KM851230 | CDC |
| Enterovirus D68 | USA/CO/2018-23087 | CO/18/23087 | B3 | MN245981 | CDC |
| Enterovirus D68 | USA/MA/2018-23089 | MA/18/23089 | B3 | MN245983 | CDC |
| Enterovirus D68 | US/KY/14-18953 | KY/14/18953 | D1 | KM851231 | ATCC (VR-1825) |
| Enterovirus 71 | 1095 | EV-A71 | N/A | U22521.1 | ATCC (VR-784) |
| Echovirus 11 | Gregory | E11 | N/A | | ATCC (VR-41) |

589

590 **Supplemental Table 2**: RT-qPCR Primers

| Primer target | Sequence-F 5'-3' | Sequence-R 3'-5' |
|---|---|---|
| CXCL10 | AAAGCAGTTAGCAAGGAAAG | TCATTGGTCACCTTTTAGTG |
| IFIT1 | CAACCAAGCAAATGTGAGGA | AGGGGAAGCAAAGAAAATGG |
| actin | ACTGGGACGACATGGAGAAAAA | GCCACACGCAGCTC |

591

592

593

594

595

596

**Figure 1**

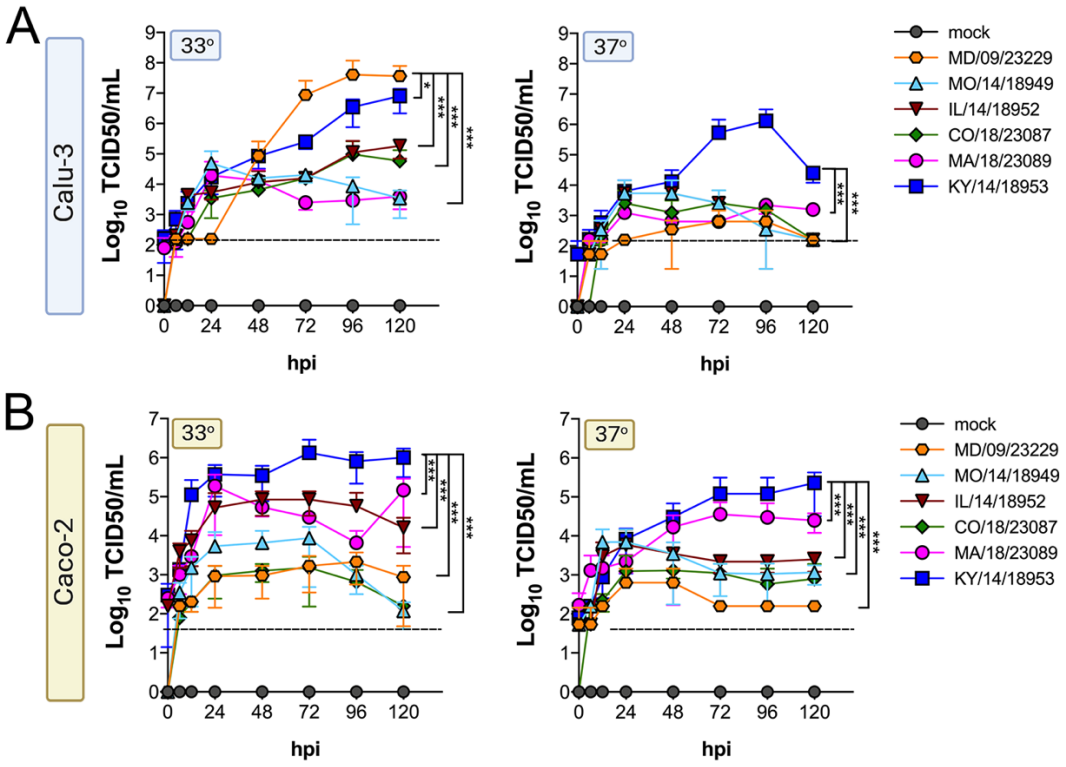


C

| Strain | Calu-3 33°C | Calu-3 37°C | Caco-2 33°C | Caco-2 37°C |
|---|---|---|---|---|
| MD/09/23229 | ++++ | - | + | - |
| MO/14/18949 | ++ | + | + | + |
| IL/14/18952 | ++ | + | +++ | + |
| CO/18/23087 | ++ | + | + | + |
| MA/18/23089 | + | - | ++ | ++ |
| KY/14/18953 | +++ | +++ | ++++ | +++ |

**Figure 1. EV-D68 replication in lung and intestinal cell lines varies with strain and temperature.** Calu-3 cells (**A)** or Caco-2 cells (**B**) were infected with the EV-D68 strains MD/09/23229 (orange), MO/14/18949 (cyan), IL/14/18952 (burgundy), CO/18/23087 (green), MA/18/23089 (pink), or KY/14/18953 (blue) at an MOI of 5 and incubated at 33°C or 37°C. The supernatant was sampled at the indicated hours post-infection (hpi) and titrated by TCID50. Data are shown as mean ± standard deviation from three replicates. Dotted line denotes limit of assay detection. **(C)**, Summary table denotes titers at 72 hpi, + corresponds to $10^3$, ++ $10^4$, +++ $10^5$, and ++++ $10^6$. Significance was determined by a Two-way ANOVA with multiple comparisons. *p<0.05, **p<0.005, ***p<0.0005, ****p<0.0001 compared to the KY/14/18953, which exhibited the highest replication levels.

**Figure 2**

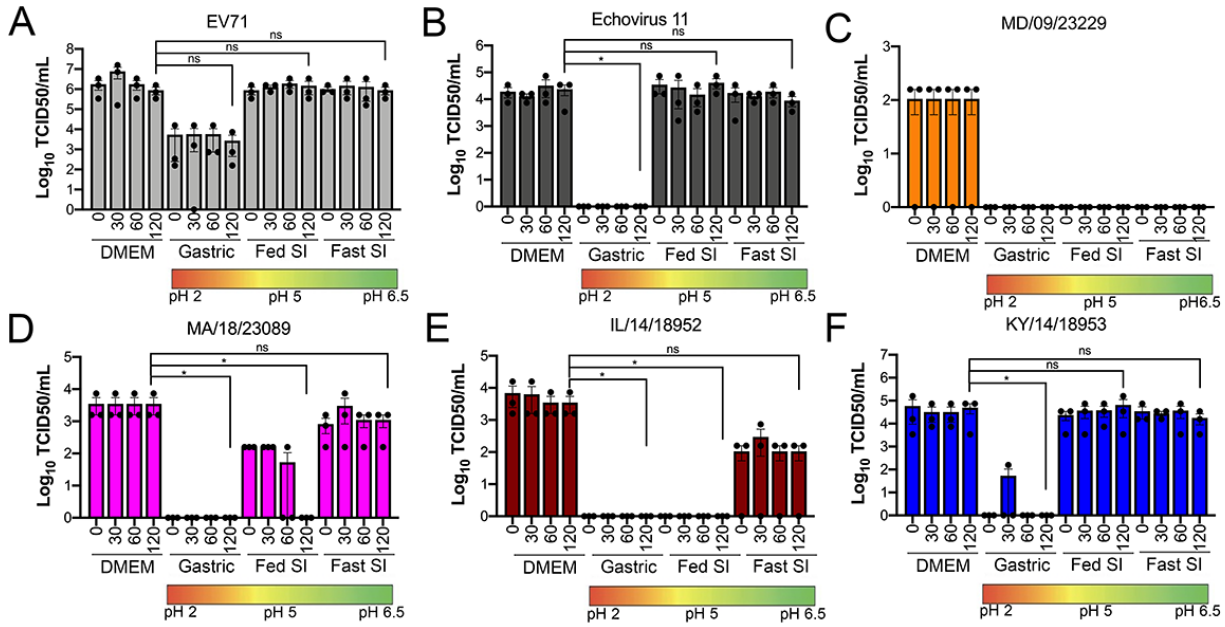


**Figure 2. Select contemporary EV-D68 strains exhibit increased acid tolerance. (A),** Enterovirus 71 (EV71), **(B),** echovirus 11 (B), or **(C-F)** the indicated EV-D68 isolates ($10^6$ PFU/mL) were incubated with control medium (DMEM), pH 2 FaSSGF (Gastric), pH 5 FeSSIF (Fed SI), or pH 6.5 FaSSIF (Fast SI) solution and incubated at 37°C for the indicated times. An aliquot of the virus/fluid mixture was collected, neutralized with sodium hydroxide, and then evaluated for infectivity via TCID50 assays. Titers are shown as mean ± standard deviation from three independent replicates. Significance was assessed at 120 min post-incubation using a One-Way ANOVA compared to DMEM-incubated controls, *p<0.05, ns, not significant.

**Figure 3**

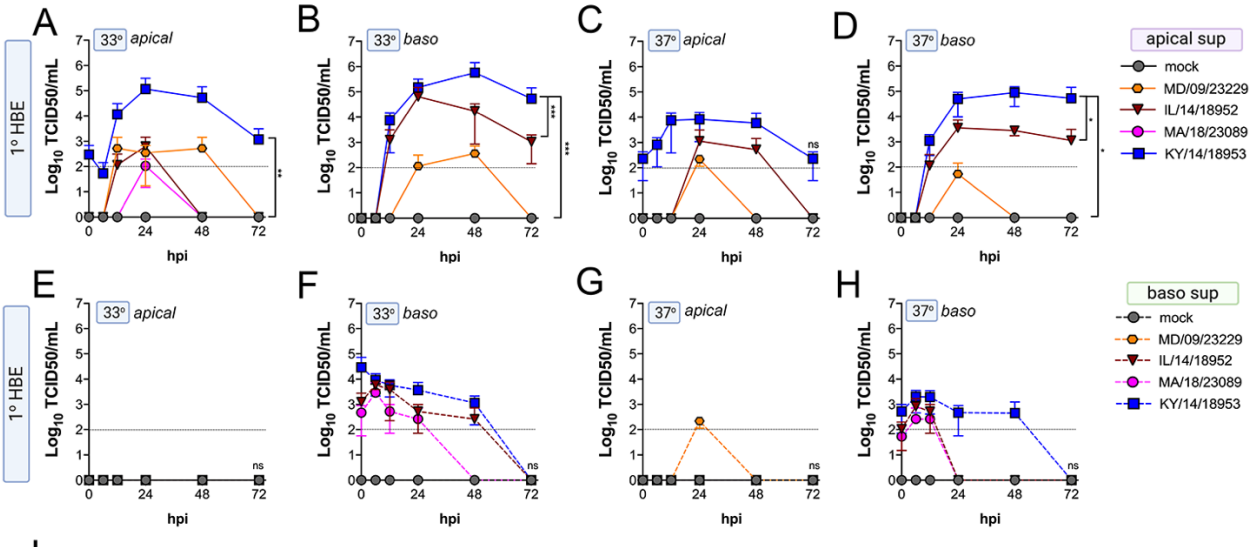


I

| Strain | HBE 33°C | HBE 37°C | HBE 33°C | HBE 37°C |
|---|---|---|---|---|
| MD/09/23229 | + | - | - | - |
| IL/14/18952 | - | + | ++ | + |
| MA/18/23089 | - | - | - | - |
| KY/14/18953 | ++ | ++ | +++ | +++ |
| Cell model/ Polarity of infection | apical | apical | baso | baso |

**Figure 3. Comparison of EV-D68 strain-specific growth characteristics in primary human airway epithelial cells.** Primary human bronchial epithelial (HBE) cells grown at an air-liquid interface were infected with $10^6$ PFU of the indicated EV-D68 strains: MD/09/23229 (orange), IL/14/18952 (burgundy), MA/18/23089 (pink), or KY/14/18953 (blue) and incubated at 33°C (**A, B, E, F**) or 37°C (**C, D, G, H**) for the indicated hours post-infection (hpi). HBE were infected from either the apical (**A, C, E, G**) or basolateral (**B, D, F, H**) surfaces. Supernatants were sampled at the indicated hpi from both apical (**A-D**) and basolateral (**E-H**) compartments and titers determined by TCID50 assays. Titers are shown as mean ± standard deviation from three independent replicates. Dotted line denotes limit of assay detection. **(I),** Summary table denotes titer at 48 hpi as collected from the apical compartment (**A-D**), - indicates no detectable replication, + corresponds to $10^3$, ++ $10^4$, +++ $10^5$, and ++++ $10^6$. Significance determined by two-way ANOVA. *p<0.05, **p<0.005, ***p<0.0005, ****p<0.0001 compared to the KY/14/18953, which exhibited the highest replication levels.

654 **Figure 4**

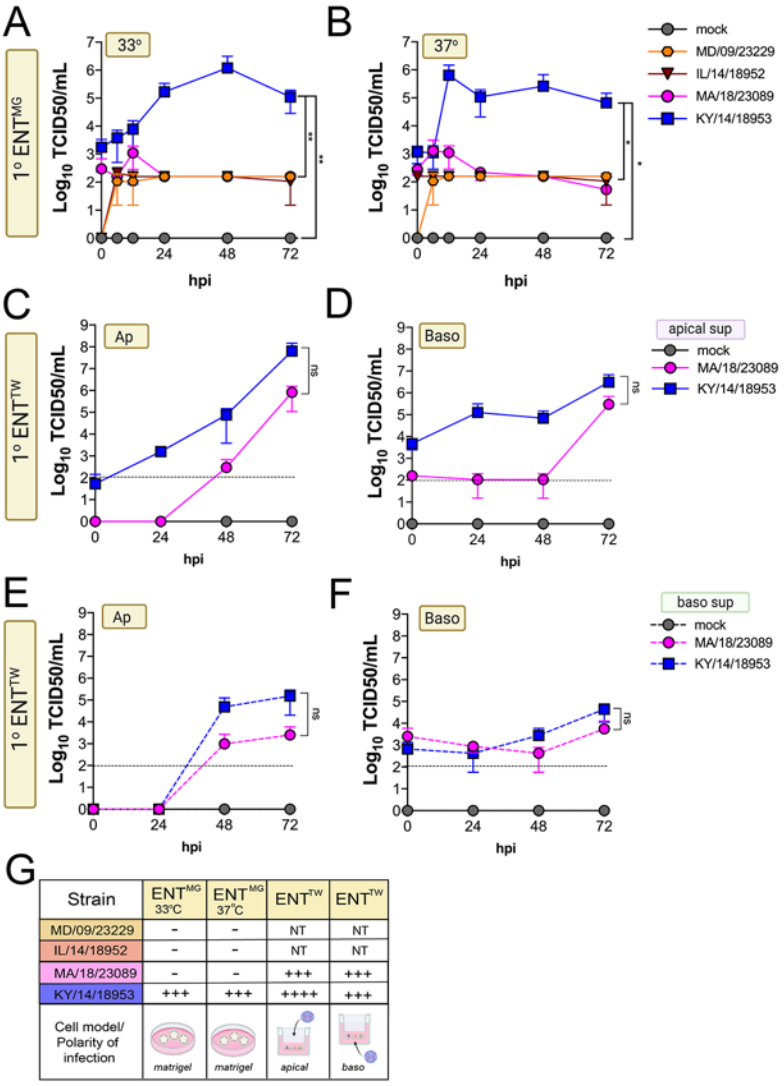


655

656 **Figure 4. Comparison of EV-D68 strain-specific growth characteristics in primary human**
657 **enteroids.** Primary enteroids grown on Matrigel (**A-B**) or transwells (**C-F**) were infected with $10^6$
658 PFU of the indicated EV-D68 strains: MD/09/23229 (orange), IL/14/18952 (burgundy),
659 MA/18/23089 (pink), or KY/14/18953 (blue) and incubated at 33°C (**A**) or 37°C (**B-F**) for the
660 indicated hours post-infection (hpi). For intestinal cells grown on transwells, cells were infected
661 from either the apical (**C, E**) or basolateral (**D, F**) surfaces. Supernatants were sampled at the
662 indicated hpi from both apical (**C-D**) or basolateral (**E-F**) compartments and titers determined by
663 TCID50 assays. Titers are shown as mean ± standard deviation from three independent
664 replicates. Dotted line denotes limit of assay detection. **(G),** Summary table denotes titer at 72
665 hpi, + corresponds to $10^3$, ++ $10^4$, +++ $10^5$, and ++++ $10^6$, NT not tested. Significance determined
666 by One-way ANOVA. *p<0.05, **p<0.005, ns, not significant.
667
668

**Figure 5**

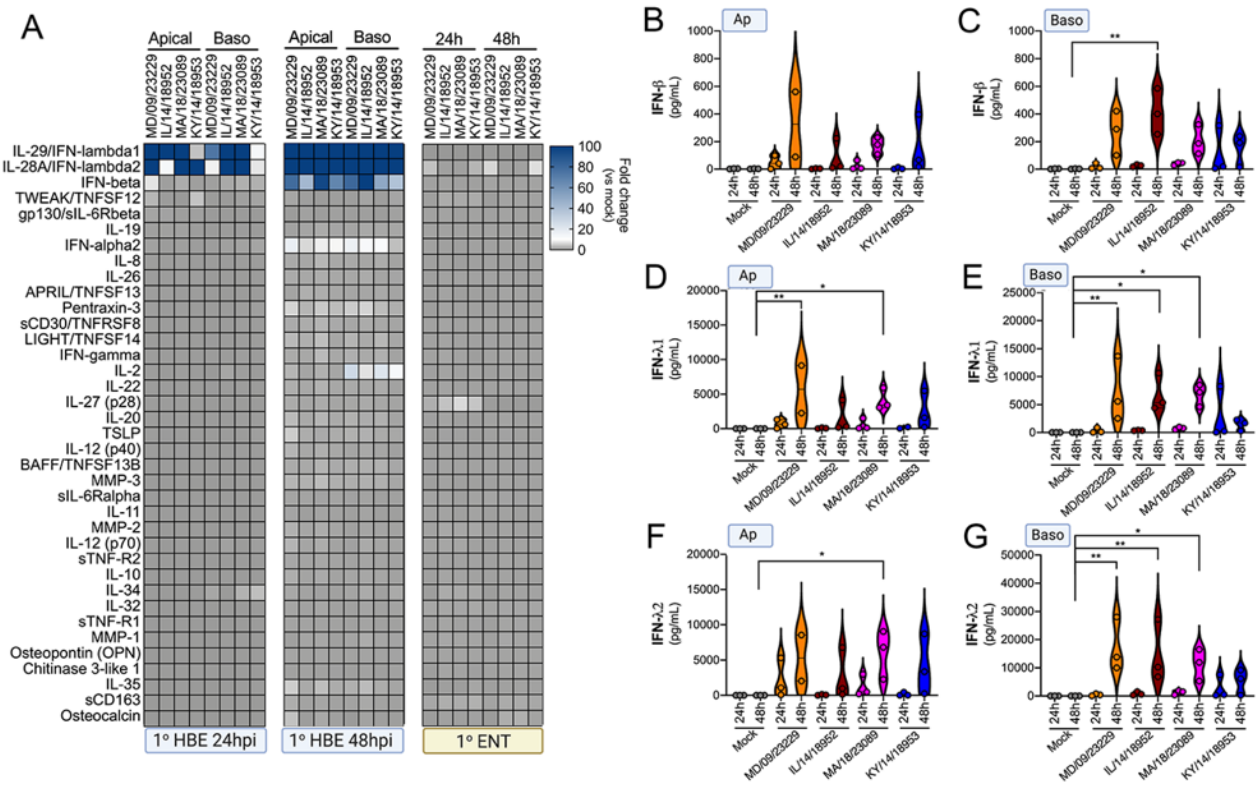


**Figure 5. EV-D68 infection of primary human airway cells induces a preferential type III IFN response. (A),** Luminex-based multianalyte profiling of 37 cytokines and chemokines in primary human bronchial (HBE) cells or enteroids (ENT) infected with $10^6$ PFU of the indicated EV-D68 strains MD/09/23229, IL/14/18952, MA/18/23089, or KY/14/18953 from the apical or basolateral surfaces and incubated at 33°C (HBE) or 37°C (ENT). Supernatants were collected from the apical compartment at 24 and 48 hours post-infection (hpi). Shown is a heatmap based on cytokines induced relative to mock infected controls (key at right), with blue denoting significantly increased cytokines in comparison to uninfected. Grey denotes little to no change (scale at top right). Data are based on three independent experiments. Levels of IFN-b **(A, C),** IFN-l1 **(D, E),** or IFN-l2 **(F, G)** infected from the apical **(B, D, F)** or basolateral **(C, E, G)** are shown. Symbols represent individual biological replicates from unique donor cells. Statistical significance was determined using a Kruskall-Wallace test, *p<0.05, **p<0.01.

690

691 **Figure 6**

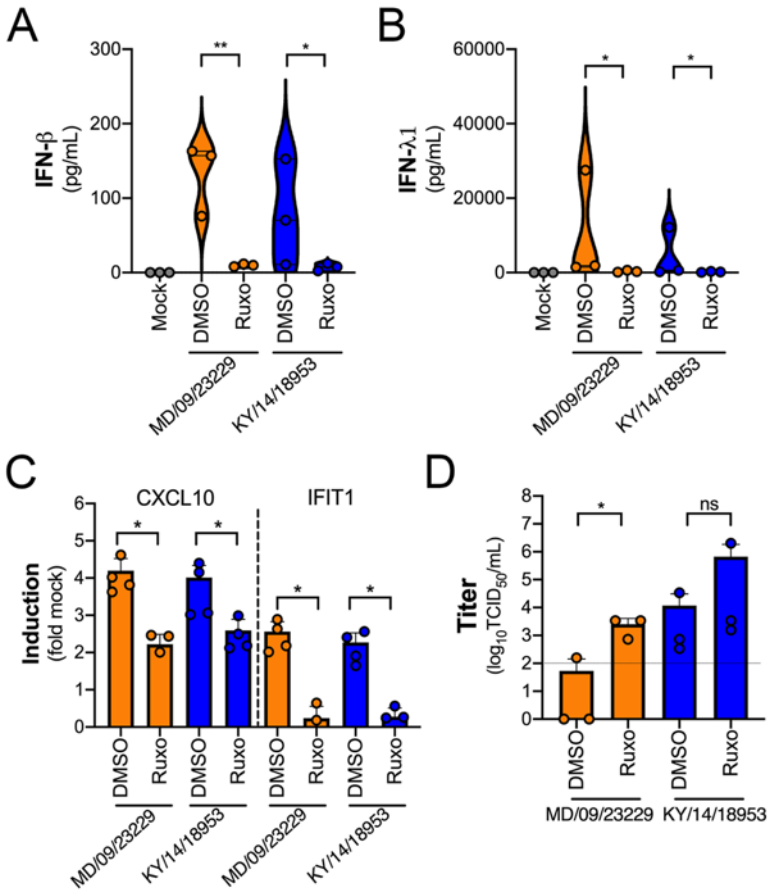


692

693 **Figure 6. IFN signaling restricts EV-D68 replication in primary human airway cells. (A,**
694 **B)** Levels of IFN-b (**A**) or IFN-l1 (**B**) as determined by Luminex-based assays in medium
695 harvested from primary human bronchial epithelial (HBE) cells pretreated with the JAK1/2 inhibitor
696 ruxolitinib **(**5 mM, Ruxo) or DMSO control for 1 hour and then infected with EV-D68
697 strains MD/09/23229 or KY/14/18953 as indicated in the presence of inhibitor for 48 hours at
698 33°C. Symbols represent individual biological replicates from at least two unique
699 donors. **(C),** Induction of the interferon stimulated genes (ISGs) CXCL10 or IFIT1 in control
700 (DMSO)- or Ruxo-treated HBE infected with the EV-D68 strains MD/09/23229 or KY/14/18953 as
701 assessed by RT-qPCR. Symbols represent individual biological replicates from at least two
702 unique donors. **(D),** Viral titers in control (DMSO) or Ruxo-treated HBE infected with MD/09/23229
703 or KY/14/18953 for 48 hours at 33°C. Statistical significance was determined using a Student's t-
704 test, *p<0.05, **p<0.01, ns not significant.
705
706

707

708

**Supplemental Figure 1**

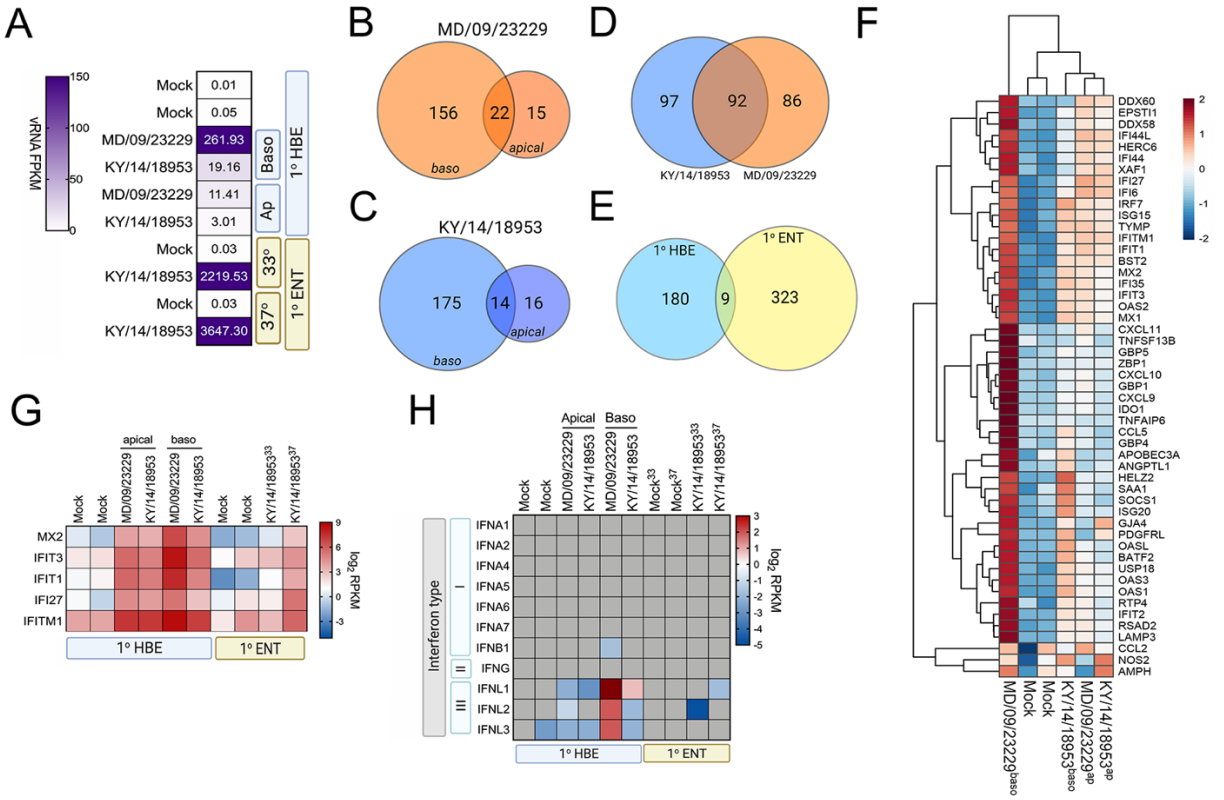


**Supplemental Figure 1. EV-D68 infection of primary human airway cells induces robust antiviral signaling.** Whole genome RNAseq-based transcriptional profiling from total RNA isolated from primary human bronchial epithelial (HBE) cells grown at an air-liquid interface or primary human enteroids infected with EV-D68 isolates MD/09/23229 and KY/14/18953 was performed in HBE infected from the apical or basolateral domains of in human enteroids infected at 33°C or 37°C. **(A)** Heatmap of vRNA FPKM (fragments per kilobase per million reads mapped) values for apical and basolateral infection of HBE with the indicated isolate and of enteroid infection at 33°C and 37°C with KY/14/18953. Key is at right. Purple indicates high viral reads and white indicates low viral reads. **(B-E),** Venn diagrams denoting the overlap in differentially regulated transcripts in HBE infected from the apical or basolateral domains with MD/09/23229 (**B**) or KY/14/18953 (**C**), shared between both isolates following basolateral infections (**D**), and between HBE and enteroids infected with KY/14/18953 (**E**). **(F)** Heatmap of select interferon stimulated genes (ISGs) in primary HBE infected with the indicated isolates of EV-D68 from the apical of basolateral domains or in mock-infected controls. Scale at right. Red indicates higher expression and blue indicates lower expression. **(G),** Heatmap of transcripts upregulated in infected HBE and enteroids by both strains based on $\log_2$ RPKM values. Key is at right. Red indicates higher RPKM values, blue represents low RPKM values, and grey represents no reads. **(H)** Heatmap of transcripts (based on $\log_2$ RPKM) associated with type I, II, or III interferons (IFNs) in HBE cells infected apically and basolaterally at 33°C with the indicated strains or in enteroids infected with KY/14/18953 at 33°C or 37°C. Scale at right, Red indicates higher RPKM values, blue represents low RPKM values, and grey represents no reads.

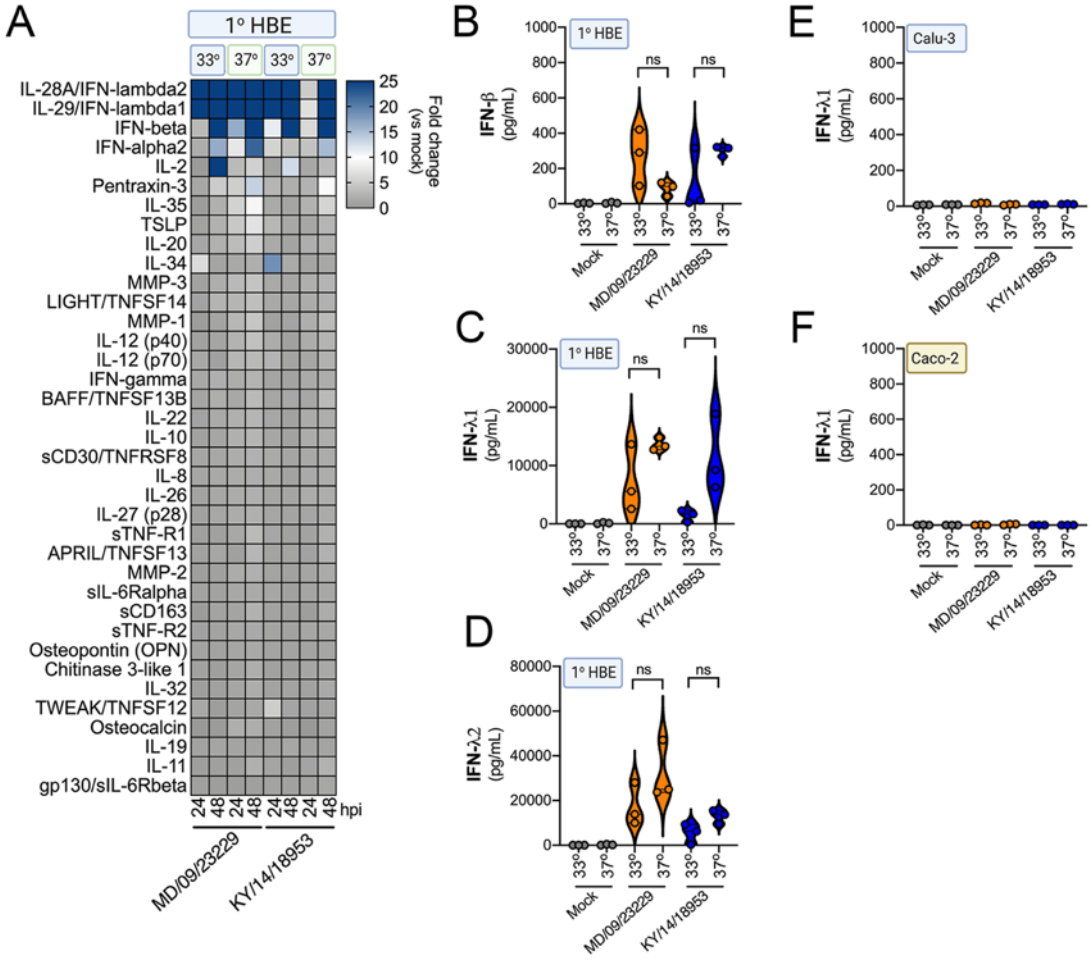


**Supplemental Figure 2. IFN induction in response to EV-D68 infection is independent of temperature.** (A), Luminex-based multianalyte profiling of 37 cytokines and chemokines in primary human bronchial (HBE) cells infected with $10^6$ PFU of EV-D68 strains MD/09/23229 or KY/14/18953 at 33°C or 37°C. Supernatant was collected from the apical compartment at 24 and 48 hours post-infection (hpi). Shown is a heatmap based on cytokines induced relative to mock infected controls (key at right), with blue denoting significantly increased cytokines in comparison to uninfected. Grey denotes little to no change (scale at top right). Data are based on three independent experiments. Levels of IFN-b **(B),** IFN-l1 **(C),** or IFN-l2 **(D)** from HBE infected at 33°C or 37°C are shown. Symbols represent individual biological replicates from unique donor cells. **(E, F),** Levels of IFN- l1 as determined by Luminex-based assays in Calu-3 (**E**) or Caco-2 (**F**) cells infected with MD/09/23229 or KY/14/18953 at 33°C or 37°C. Symbols represent individual biological replicates. Statistical significance was determined using a Student's t-test, not significant (ns).